arXiv:1303.1405v1 [cond-mat.soft] 6 Mar 2013

Plastic flow in a sheared polycrystalline solid using phase field model

Santidan Biswas[1], Martin Grant[2], Indradev Samajdar[3], Arunansu Haldar[4], and Anirban Sain[1]*
[1] *Department of Physics,* [3] *Department of Metallurgical Engineering and Materials Science,*
Indian Institute of Technology, Bombay, Powai, Mumbai-400 076, India.
[2] *Department of Physics, McGill University, Rutherford Building, Montreal H3A 2T8, Canada.*
[4] *Research and Development, Tata Steel, Jamshedpur 831007, India.*
(Dated: March 7, 2013)

Plastic deformation in solids induced by external shear stress is of huge practical interest. Presence of local crystalline order in polycrystals, consisting of many grains, distinguishes its deformation pattern from that of amorphous materials. Despite strong anisotropy, induced by external stress, the plastic flow and the consequent deformation field show strong dynamical heterogeneity. The distribution $P(u)$ of particle displacements (u) shows three distinct regimes including a power law scaling regime at moderate displacements. Using a phase field simulation we show how polycrystals generate saddle and vortex like flow patterns, which hitherto have been termed as elementary plastic events in the context of amorphous materials. Interestingly, such events here find natural explanation in terms of the underlying dislocation dynamics. We also characterize the spatial distribution of the flow field using Okubo-Weiss measure.

PACS numbers:

Solids undergo plastic deformation and subsequently flow when they are subjected to stresses beyond their elastic limit. Understanding plastic flow in polycrystalline solids has huge practical importance, starting from applications in material processing to understanding earthquake dynamics. Metals are deformed routinely in various industrial applications, for example, by rolling or pressing them into sheets. In earthquake dynamics, it is the shear stress generated by the movement of tectonic plates which causes plastic flow. Such deformations and flows under constant shear stress as well as constant shear strain rates have been widely studied both by lab experiments [1] and simulations [2]. Experiments on crystalline ice has established that acoustic emission which is a signature of dislocation avalanches in stressed solid is strongly intermittent and shows power law distribution of the energy released by such activity. Simulations using dislocation dynamics model and crystal phase field models have reproduced this [1, 2]. Simulation of amorphous solids [3–5] has also shown signature of spatially intermittent behavior which often organize into large flows in the form of vortices and saddles.

Plastic flow in a polycrystal ranges over multiple length scales starting from the motion (glide/climb) of single dislocations at the nanometer scale to movement of grain boundaries at micron and larger scales. Also they are highly anisotropic biased by the direction of the macroscopically applied external stresses. We are interested in the nonequilibrium dynamics of the plastic flow which is generated when the solid is subjected to external shear stress. While most studies have discussed the displacement field which results from a quasi-static strain [3–5], we subject the solid to a constant strain rate [2].

We employ phase field crystal (PFC) model to simulate a sheared polycrystalline solid in two dimensions. The strength of the phenomenological PFC model [6, 7] is that it can study dynamics of crystalline solids at the microscopic (atomic) length scales but diffusive time scales (much longer than vibrational time scales). Also here dislocations are generated spontaneously without any ad-hoc rules being imposed. PFC model have been augmented (modified PFC) with an acceleration term in the damped Langevin equation. This reintroduces the fast acoustic waves into the dynamics. PFC and modified-PFC have been successful in reproducing important phenomenology of grain-boundary energy [8], premelting transition [9], dislocation glide [10] to mention a few. It has also been applied to study glass transition time scales [11] and liquid crystal dynamics [12]. Modified PFC has also been derived [8] from microscopic density functional theory.

We confine the square shaped solid between two parallel plates, at $y = 0$ and $y = 2H$ which are moved at uniform speeds $v_0\hat{x}$ and $-v_0\hat{x}$, respectively. Along the x direction we apply periodic boundary condition. To simulate the dynamics we use the modified phase field crystal (MPFC) model developed in Ref[11,17] and follow a shearing scheme proposed by Chan et al. [2]. The dimensionless equation of motion of the system is as follows :

$$\frac{\partial^2\psi}{\partial t^2} + \beta\frac{\partial\psi}{\partial t} = \alpha^2\nabla^2(\omega(\nabla^2)\psi + \psi^3) + v(y)\frac{\partial\psi}{\partial x} + \zeta, \quad (1)$$

where ψ is the conserved order parameter field, $\omega(\nabla^2) = r + (1+\nabla^2)^2$ and ζ is the conserved noise. α, β variables control the time scale of the phonon modes propagating in the solid and the degree of their damping. In this shearing scheme instead of moving only the top and the bottom surfaces of the solid, a drift velocity profile, $v(y)\hat{x} = v_0\exp(-y/\lambda)$ for $0 < y < H$ and $v(y)\hat{x} = v_0\exp(-(2H-y)/\lambda)$ for $H < y < 2H$, that decays exponentially away from the surface (towards the bulk) is applied on the solid. We hope that as long as the length scale of decay $\lambda \ll H$, the width of the solid, the physics in the bulk will not be affected by λ. We examined the effect of this imposed drift by measuring the average velocity along the flow direction, $|\langle v_x(y)\rangle|$ as a function of y (see inset of Fig.1-c) and inferred that there exists a sizable bulk portion. All our studies focus on this bulk region.

The results presented here are from simulations on a square grid of size 256×256. No qualitative difference was found for a bigger grid (1024×1024), except that the data is much better averaged for the presented case due to reasonable run time. The parameters used are $H_x = H_y = 256$, $\alpha = 1$, $\beta = 1$, $\lambda = 10$, $\psi_0 = 0.3$, $r = -0.5$, $dx = 3\pi/8$, $v_0 = 0.45$ and $dt = 0.025$. Note that our λ/H_y is half of that in Ref[2]. We used a pseudo-spectral scheme, combined with integrating factor method, to solve the PDE in Eq. 1. We used two different initial conditions: a) a single crystal and b) a random distribution of grains of different sizes, grown by implanting many artificial nuclei in the supercooled liquid state. Under constant strain rate both led to the same (statistically) nonequilibrium, steady polycrystalline state with relatively smaller grains near the boundaries than in the interior (see Fig.1-a).

In PFC model, the particles are identified as the minima of the scalar field $\psi(\mathbf{r}, t)$. The grains have triangular lattice structure (see Fig.1.1-a), typical of 2D, with the local orientation field given by the angle $\theta(\mathbf{r}) \in [0, \pi/3]$. The maximum misorientation between two neighboring grains can be $\pi/6$. Local crystal orientation at each particle was obtained from the positions of its neighbors and keeping in mind the triangular symmetry of the crystal. At grain boundaries crystal orientation changes. Using Delaunay triangulation, the number of nearest neighbors of each atom and the specific atoms linked to it was obtained. Dislocations were located by finding pairs of atoms with 5 and 7 neighbors on the Delaunay network.

As mentioned in the introduction, collective motion in response to small shear strain applied at the boundaries of a solid [3–5], has been studied for amorphous material. But since the applied strain there [3–5] was quasistatic in nature (keeping the system always at equilibrium or at worst metastable equilibrium), the motion was athermal (i.e., $T = 0$). In contrast here we study the actual temporal dynamics in response to a constant strain rate. Collective motion of a many body system is often interpreted as the motion Under a constant strain rate, as ours, the system has no time to settle down in the local minima consistent with the global strain. The landscape changes at a much faster time scale compared to the relaxational kinetics of the system. Thus the collective motion is nonequilibrium in nature and we focus on the steady state features.

Several new features arise because of the polycrystalline nature of the sheared solid. The grains do not transmit hydrodynamic stresses from one part of the system to the other like a fluid or even like an amorphous solids. A grain resists motion till the accumulated strain crosses its elastic limit and then either rotate with respect to its neighboring grains or break up into smaller grains. Therefore the scale of motion is controlled by the typical grain size, which becomes smaller at higher strain rates. Fig. 1-b shows the detailed velocity map of the particles in the bulk. Despite the strong bias along $\hat{x}$ (the shear direction) the flow field shows significant motion along $\hat{y}$, giving rise to characteristic vortical and saddle type of motion as shown in Fig. 1-b. Origin of such kind of motion will be discussed later. The inset of Fig. 1-c shows $\langle v_x(y) \rangle$ as a function of y, which shows an emergent velocity profile in the bulk differing from the imposed drift velocity. Despite the shear induced anisotropy the flow is highly heterogeneous even within the bulk: very slow in the interior of the grains and fast at the grain boundaries. Since flows are driven by local stresses, high shear stresses are expected at the grain boundaries which we will discuss next. The plastic flow also results in interesting displacement patterns which will be discussed later.

Large scale molecular dynamics (MD) simulations on sheared amorphous material [3–5] have demonstrated that plastic displacement patterns organize into large scale vortices when the externally imposed, global, shear strain is changed quasi-statically. Ref. [4] has shown that an elementary, irreversible, plastic event is a quadrupolar displacement pattern which has long range elastic effect. Picard et al [14], studied the effect of a localized plastic event in a sheared 2D viscoelastic medium. They analytically showed how, through elastic interaction, it induces a long range strain field which turns out to of quadrupolar nature. The event was assumed to be a localized plastic strain $\epsilon_{ij}\delta(\mathbf{r})$ corresponding to a pure shear deformation, i.e., only the non-diagonal elements of ϵ_{ij} were non-zero and equal. Generation of such a plastic strain matrix is at best plausible given the material is being globally sheared through its external boundaries. The MD simulations of Maloney and Lemaitre [3, 4] on 2D sheared amorphous materials could nail down such local plastic events to characteristic motion of particles near a saddle with one stable and another unstable axis, and particles move towards and away, respectively, from the saddle along these axes. But it is still unclear how such singular points are created in the interior of the system due to global shear stress applied at its distant boundaries.

We identify a microscopic mechanism which can dynamically give rise to quadrupolar patterns, essentially a saddle, in the displacement field of the particles. We show that such a pattern results from sideways approach of two oppositely charged edge dislocations towards each other. The sequence in Fig. 2 clearly shows time development of the displacement field leading towards a saddle as the dislocations approach each other. The saddle fades away after the dislocations annihilate (not shown here). Such long range quadrupolar patterns have been reported for noncrystalline (amorphous) material [4] also, but there being no dislocations in noncrystalline material microscopic origin of such a quadrupolar pattern remained unexplained. Quantitatively we know that the displacement field of an edge dislocation generates a displacement dipole where the positive and negative lobes are oriented along the axis connecting the atoms with coordination numbers 5 and 7. Such a $5-7$ pair is like a charge dipole and sideways arrangement of two such pairs form a quadrupole. Essentially these two dislocations have opposite burgers vectors $\vec{b}$ and $-\vec{b}$ along one of the symmetry axes of the crystal. In comparison, dislocations with the same burgers vector can line up in an "..5-7-5-7-5-7.." arrangement to form a dislocation wall (see Fig. 1-a) which is rather stable. These walls are equivalent to high angle grain boundaries (Fig. 1-a). The

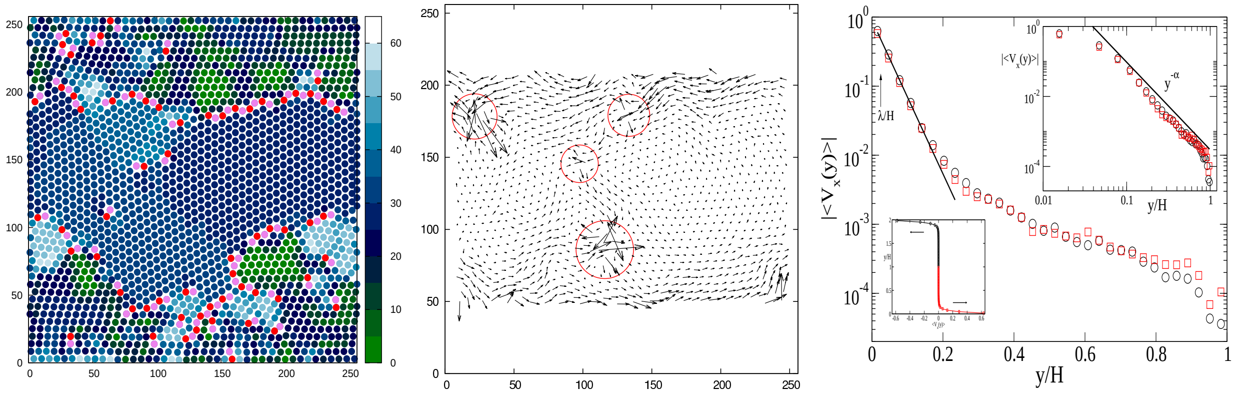

FIG. 1: (Color online) (a) Spatial map of the local crystal orientation $\theta(\mathbf{r})$ with a range $[0, \pi/3]$. Dislocations are indicated by light colors. They decorate the grain boundaries separating grains with high misorientation. Across grains with very low misorientation (cells) they are absent. This is consistent with the Frank condition ($n \propto \sin\theta$) [13], which relates the line density of dislocations (n) along a grain boundary and the corresponding misorientation angle (θ). (b) Velocity pattern of the particles in the bulk. Velocities near the moving boundaries are too large in magnitude to be represented in the same plot. Vortices are visible near the top and bottom boundaries while saddles (circled) are visible in the bulk. We omitted the velocity pattern near the boundary region since the velocity scale is much higher there compared to the bulk. (c) Shows shows semi-log plot of $\langle v_x(y)\rangle$ as a function of y. To bring out the anti-symmetry of the average flow with respect to the mid-plane ($y = H$), we reflected $\langle v_x(y)\rangle$ for $y < H$ across the mid-plane and then used modulus (increasing y is directed towards the bulk. The solid line shows the imposed drift velocity $v(y) \sim v_0 \exp(-\lambda/y)$. The upper inset shows the same data in a log-log plot which brings out the scaling behavior $y^{-\alpha}$ in the bulk. The lower inset shows the same data in a regular $x - y$ plot.

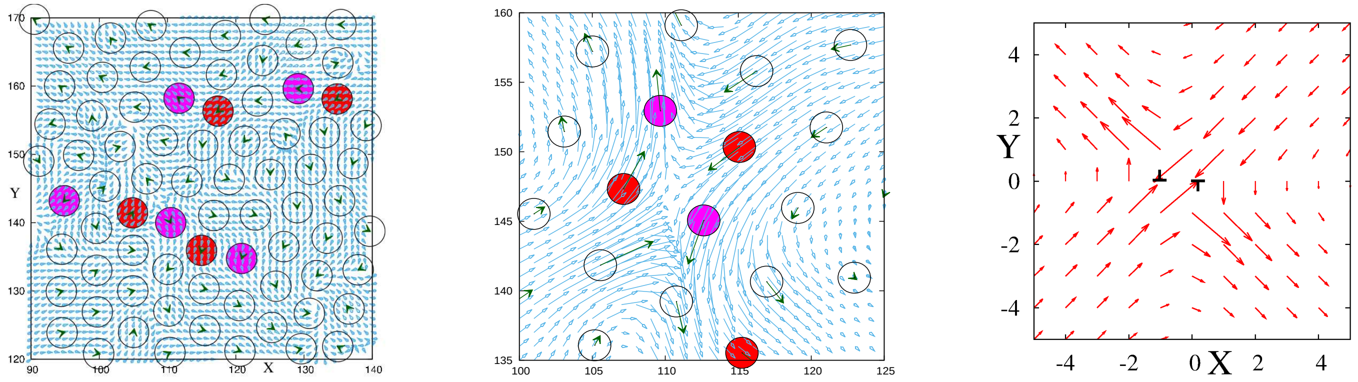

FIG. 2: (a) and (b) focus on a small region of the lattice. The circles represent the atoms and the dark arrows on the circles represent their velocity vectors while the light arrows represent the interpolated velocity field. The filled circles are the atoms with five or seven neighbors, indicating an edge dislocation. (a) shows initiation of a saddle as two oppositely charged dislocations approach. (b) Time development of the saddle as the dislocations get close to form a quadrupole. Note that 'b' has higher resolution than 'c'. (c) The superposed displacement field of two edge dislocations (with opposite Burgers vector) calculated using Eq. (2). The parameters used are $b = 1$ and $\nu = 0.1$. The dislocation positions are $(0, 0)$ and $(-1, 0)$.

quadrupolar structure discussed above can be quantitatively established by superimposing the elastic displacement fields of two dislocations located close by. Fig. 2 shows the resultant field from two dislocations located at $\vec{r} = (0, 0)$ and $(-1, 0)$, where displacement field $\vec{u}(\mathbf{r})$ due to a dislocation at the origin is given by [15]

$$\begin{aligned} u_x &= \frac{b}{2\pi}\left[\tan^{-1}\frac{y}{x} + \frac{xy}{2(1-\nu)(x^2+y^2)}\right], \\ u_y &= -\frac{b}{2\pi}\left[\frac{1-2\nu}{4(1-\nu)}\ln(x^2+y^2) + \frac{x^2-y^2}{4(1-\nu)(x^2+y^2)}\right] \end{aligned} \quad (2)$$

where ν is the Poisson ratio and $\tan^{-1}\frac{y}{x} \in [0, 2\pi]$. It is worth mentioning that we have found saddle structures in the displacement profile even in places where there are no dislocations. Thus the above mechanism cannot be the only reason for saddles.

In order to study the spatial distribution of vorticity and saddles (centres) in our 2D plastic flow we employ a technique borrowed from fluid turbulence [16, 17]. For 2D inviscid, incompressible flows the OkuboWeiss parameter is defined as $\lambda = \det(\partial_i v_j)$. This is an invariant of the flow and can be recast as $\lambda = \omega^2 - \epsilon^2$, where $\vec{\omega} = \vec{\nabla} \times \vec{v}$ is the vorticity vector and $\epsilon^2 = \sum_{i,j} \epsilon_{ij}^2$, where $\epsilon_{ij} = (\partial_i u_j + \partial_j u_i)/\sqrt{2}$ is

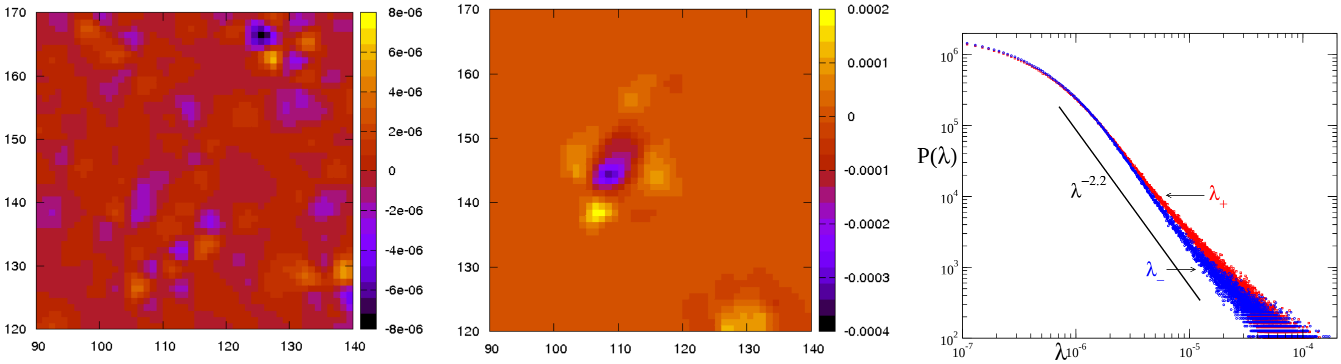

FIG. 3: (a) Okubo-Weiss field $\lambda(x, y)$ in the bulk, corresponding to the velocity fields a and b of Fig.2. (b) clearly shows the prominent saddle (violet) and the surrounding vorticity field (yellow). Note that, in (a) also many saddles (violet) are visible but their intensity is two order of magnitude weaker than that in (b). (c) Log-log plot of the distribution of the Okubo-Weiss field. We show separate PDFs' for the positive (vorticity) and negative (extensional) values of λ, indicated by λ_+ and λ_- respectively ($\lambda_- = |\lambda|$ when $\lambda < 0$). The PDFs' are nearly symmetric and has power law regimes.

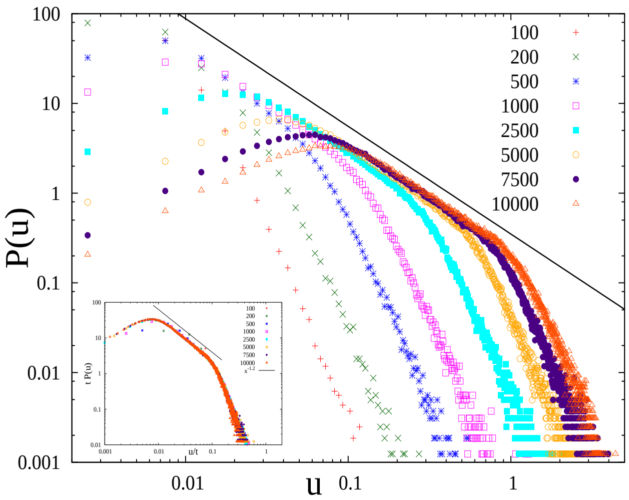

FIG. 4: Distribution of displacement magnitudes of all the particles, collected after different time intervals t (shown in arbitrary units in the figure). The inset shows data collapse of the plots shown in after rescaling u by t, and $P(u)$ appropriately. This collapse is possibly a consequence of the fact that the average $x-$displacement $\langle u_x \rangle = \langle v_x \rangle t$ dominates the behavior of u. But the scaling behavior cannot be explained by this. The scaling exponent is -1.2 and the plots for large t only show significant scaling regimes.

the strain tensor. Even in viscous flows λ turns out to be an useful measure and regions with vortices have $\lambda > 0$, while the strain dominated regions have $\lambda < 0$. Note that a saddle correspond to stretching in one direction and compression in the orthogonal direction, i.e., it generates a strain dominated region.

Our system is not strictly incompressible, so we computed the incompressibility parameter $\kappa = \langle(\vec{\nabla}.\vec{v})^2\rangle/\langle(\vec{\nabla}\vec{v})^2\rangle$, where the denominator is essentially $\sum_{i,j}(\partial_i v_j)^2$. For an incompressible fluid the numerator is zero, while our system yields a value of $\kappa < 0.2$ (averaged over many configurations), which is small enough for an incompressibility approximation to be valid. Also in terms of total particle numbers, the fluctuation is less than 1% (less than 20 in 2000). For computing κ we interpolated the particle velocities onto a square grid. In Fig3-a,b we plot the Okubo-Weiss field corresponding to the velocity fields (a and b) of Fig.2. We also compute the distribution function of λ, shown in Fig.3-c.

Finally we report intriguing power laws in the PDF of the particle displacements $|\vec{u}_j|$, in the bulk (excluding the boundary region where $\langle v_x(y) \rangle$ is exponential). Here j is the particle index. It turns out that although velocity of the particles, $\vec{v}_j$, are quite random, the displacements $\vec{u}_j$ after large time intervals show characteristic patterns, around the plastic events (figure not shown here). The PDF of $u \equiv |\vec{u}_j|$ is shown in Fig. 4, which, at large time intervals t, shows two clear power law regimes. Rescaling u with t (and also $P(u)$ appropriately) the PDFs' collapse nicely (inset of Fig.4), although the PDFs' for short t do not have any power law regime.

The different scaling regimes of $P(u)$, namely, $\propto u$ and $\propto u^{-1.2}$, reflect distinct kind of particle motion in the sheared polycrystal. $P(u)$ is the fraction of particles undergoing particular type of motion and is therefore approximately proportional to the area fraction occupied by these particles in a typical velocity map like Fig.2b. The displacements are small at the core of the large grains where motion is vortical. Assuming a slow rotational speed ω_0, the displacement u, for $\omega_0 t \ll 1$, is $u \sim \omega_0 r t$, where the radius r is measured with respect to the center of the grain. Thus $P(u)du \propto dA = 2\pi r dr$ and using $u \sim \omega_0 r t$, we get $P(u) \sim u\frac{2\pi}{(\omega_0 t)^2}$. Consequently a time independent collapse occurs in the $P(u)t$ versus u/t plot (inset of Fig.4). Larger displacements (the $u^{-1.2}$ regime) are dominated by $\langle v_x \rangle$ and here approximately $\langle v_x(y) \rangle \sim y^{-3}$ (log-log plot of $\langle v_x(y) \rangle$ versus y not shown here). Now in this case $P(u)du \propto dA = dy.L$ and using $u \sim y^{-3}t$, we get $tP(u) \sim \frac{1}{3}(\frac{u}{t})^{-4/3}$; again a t independent collapse. Although our $P(u)$ is restricted to the bulk region, any remnant effect from the boundary region, where $\langle v_x(y)\rangle$ is exponential, would contribute a u^{-1} scaling. The observed $u^{-1.2}$ scaling is possibly a mixed effect.

In summary, we have shown that the plastic flow in sheared polycrystals show strong dynamical heterogeneity which manifests as three distinct regimes in the displacement distribution of the particles. Further, the elementary plastic events of the flow field can be explained in terms of the underlying dislocation dynamics. That bridges two seemingly disparate descriptions, namely continuum and discrete, of sheared solids.

---

[*] Electronic address: asain@phy.iitb.ac.in

[1] M.-C. Miguel, A. Vespignani, S. Zapperi, J. Weiss, and J.-R. Grasso, Nature **410**, 667 (2001).
[2] P. Y. Chan, G. Tsekenis, J. Dantzig, K. A. Dahmen, and N. Goldenfeld, Phys. Rev. Lett. **105**, 015502 (2010).
[3] C. Maloney and A. Lemaitre, Phys. Rev. Lett. **93**, 016001 (2004).
[4] C. Maloney and A. Lemaitre, Phys. Rev. Lett. **93**, 195501 (2004).
[5] A. Tanguy, J. P. Wittmer, F. Leonforte, and J.-L. Barrat, Phys. Rev. B **66**, 174205 (2002).
[6] K. R. Elder, M. Katakowski, M. Haataja, and M. Grant, Phys. Rev. Lett. **88**, 245701 (2002).
[7] P. Stefanovic, M. Haataja, and N. Provatas, Phys. Rev. Lett. **96**, 225504 (2006).
[8] K. R. Elder and M. Grant, Phys. Rev. E **70**, 051605 (2004).
[9] J. Berry, K. R. Elder, and M. Grant, Phys. Rev. B **77**, 224114 (2008).
[10] J. Berry, M. Grant, and K. R. Elder, Phys. Rev. E **73**, 031609 (2006).
[11] J. Berry and M. Grant, Phys. Rev. Lett. **106**, 175702 (2011).
[12] R. Wittkowski, H. Löwen, and H. R. Brand, Phys. Rev. E **82**, 031708 (2010).
[13] W. T. Read and W. Shockley, Phys. Rev. **78**, 275 (1950).
[14] G. Picard, A. Ajdari, F. Lequeux, and L. Bocquet, Eur. Phys. J. E **15**, 371 (2004).
[15] S. Timoshenko, *Theory of Elasticity* (McGraw-Hill, 1951).
[16] J. Weiss, Physica D **48**, 273 (1992).
[17] P. Perlekar and R. Pandit, New J. Phys. **11**, 073003 (2009).